Regioselectivity control in Pd-catalyzed telomerization of isoprene enabled by solvent and ligand selection

Jordi Colavida,[a] José A. Lleberia,[b] Antoni Salom-Català,[b] Aitor Gual,[a] Ana Collado,[c] Ennio Zangrando,[d] Josep M. Ricart,[b] Cyril Godard,[b] Carmen Claver,[a,b] Jorge J. Carbó,*[b] and Sergio Castillon*[a,e]

[a] CTQC-Eurecat-UTQ, C/Marcel·lí Domingo 2, building N5, 43007 Tarragona, Spain.
[b] Department de Química Física i Inorgànica, Universitat Rovira i Virgili, C/Marcel·lí Domingo 1, 43007 Tarragona, Spain.
[c] International Flavors and Fragrances, Av/Felipe Klein 2, 12580 Benicarló, Spain.
[d] Dipartimento di Scienze Chimiche e Farmaceutiche, University of Trieste, Via L. Giorgieri 1, 34127 Trieste, Italy.
[e] Department de Química Analítica i Química Orgànica, Universitat Rovira i Virgili, C/Marcel·lí Domingo 1, 43007 Tarragona, Spain.

KEYWORDS Telomerization; non-symmetric dienes; isoprene; regioselectivity; mechanism; palladium; solvent control; ligand control

ABSTRACT: Controlling the selectivity in palladium-catalyzed telomerization of non-symmetric dienes represents a formidable challenge since up to 12 isomers can be obtained, and a general method for selective synthesis is still lacking. We select isoprene (2-methylbutadiene) as a representative and relevant example of non-symmetric diene. A combined experimental-computational study on a large set of phosphine-modified palladium catalysts and reaction conditions aiming to understand the factors governing the selectivity shows that it can be controlled by selecting the protic solvent pKa and by the ligand. Atomistic and kinetic simulations reveal that the solvent switches the selectivity-determining step as function of pKa, from C-C oxidative coupling at low pKa values (preference for telomer head-to-head) to protonation at high pKa values (preference for telomer tail-to-tail). The selectivity towards tail-to-head telomer can be directed in moderately acidic solvents by the selection of the appropriate ligand, which exerts a steric control of the protonation step. Thus, using Et_2NH as nucleophile, it was possible to synthesize 3 of the 4 main isomers in very high yields and selectivities and to provide a complete mechanistic picture of Pd-catalyzed telomerization of non-symmetric dienes.

INTRODUCTION

The telomeriation of dienes, first disclosed by Smutny[1] and Takahashi[2] in 1967, consists of the dimerization of a diene catalyzed by a transition metal with subsequent addition of a nucleophile, such as an alcohol, an amine, an acid, and water, to form highly valuable intermediates.[3,4,5,6,7,8] Butadiene is the most simple and widely studied substrate, and its telomerization can afford three different products, with the linear telomer presenting the most interesting properties (Scheme 1).[3] Butadiene telomerization[9,10,11] is today an industrial process key for 1-octene production.[11]

The mechanism of butadiene telomerization[12,13,14,15] involves four different steps (Scheme 1): (1) reduction of Pd^{2+} precursor to Pd^0 and coordination of two butadienes (A), (2) oxidative butadiene coupling (B), (3) protonation at the C6-position (C), and (4) nucleophilic attack (D)(Scheme 1). DFT calculations[16,17] completed the mechanistic picture for butadiene telomerization with methanol and trimethylamine as the base, and proposed that protonation is fast and Me_3NH^+ species acts as a proton source,[17] although the energy cost of its formation was not evaluated.

Despite the interest in the telomerization of non-symmetric dienes, this reaction has been infrequently used due to regioselectivity issues. For isoprene, the simplest example of non-symmetric diene and that provides an easy entry to monoterpenes, the telomerization process can yield up to 12 isomers, making this process a formidable challenge. To date, the mechanism of non-symmetric diene telomerization has been scarcely studied,[12] despite of its crucial importance for the development of selective catalysis. Beller *et al.* proposed for isoprene a mechanism similar to butadiene (Scheme 1) but with four parallel catalytic cycles, each providing one of the main linear telomers 1-4.[18] Nevertheless, the factors determining the selectivity have not been identified yet and remain unknown.

Scheme 2a summarizes the efforts made in palladium-catalyzed telomerization of isoprene with Et_2NH, aiming to obtain the main telomers selectively. Thus, using [Pd(η^3-C_3H_5)COD]BF_4/P(2,4,6-tri-OMe-Ph)$_3$ as catalytic system a selectivity of 96.6% in head-to-head telomer **2** was obtained.[19] Excellent selectivities in tail-to-head (**1**) and tail-to-tail (**3**) telomers were also reported, although the activities were very poor.[20,21] Selective formation of telomer **3** (81%) employing [Pd(C_3H_5)COD] BF_4/P(OBu)$_3$ as catalytic system was also reported.[20] Telomer head-to-tail (**4**), not

included in Scheme 2a, was always obtained with low selectivity. These results illustrate the difficulty of obtaining both high yield and high selectivity in isoprene telomerization, and in general in non-symmetric dienes telomerization, probably because factors controlling the selectivity of the reaction have not been stablished.

Scheme 1. Pd-Catalyzed butadiene telomerization and proposed mechanism.

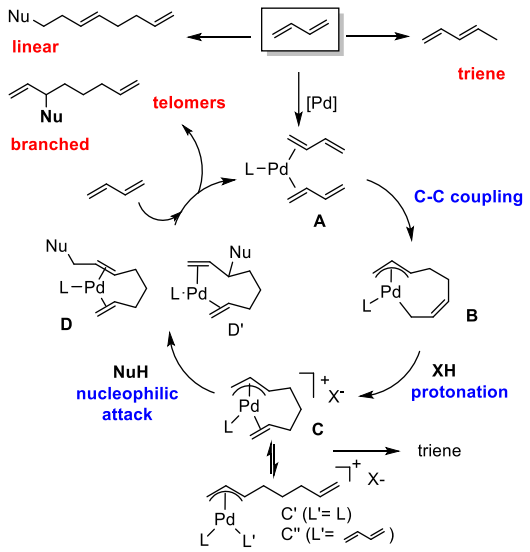

Scheme 2. a) Isoprene telomerization main reported results. b) This work

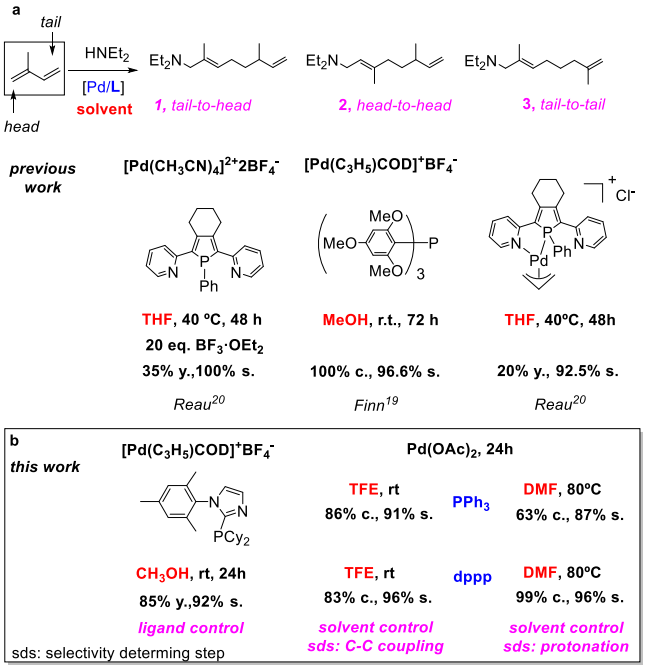

In this context, the general understanding of the parameters affecting the catalytic cycle and the search for efficient catalytic systems providing linear telomers in good yield and selectivity, are of high interest from both academic and industrial perspectives. Here, we report that the selectivity of isoprene telomerization is determined by both the solvent and the ligand, which has allowed us to find Pd/ligand/solvent catalytic systems for isoprene telomerization with Et_2NH that provide telomers **1**, **2** and **3** in high yields and excellent selectivities (>90%) (Scheme 2b).[22] Atomistic DFT calculations in combination with kinetic simulations allowed for the first time the understanding of the role of solvent and ligand and provided a complete mechanistic picture of this challenging reaction.

RESULTS AND DISCUSSION

Catalysis

Initially, we assessed the influence of different parameters on the selectivity. First, we evaluated the effect of solvents by systematically varying their acidity from 2,2,2-trifluoroethanol (TFE) (pKa= 12.4) to *tert*-butanol (tBuOH) (pKa=19.2) (see Table 1). The reactions of isoprene with Et_2NH were performed using $Pd(OAc)_2/PPh_3$ (**P1**), and Pd/L (1:1.5) (see SI, Tables S1-S18, for reaction optimization). Interestingly, the results showed a progressive shift of selectivity from **1**+**2** to **3**+**4** upon going from TFE to tBuOH, while the yield decreased concurrently. Specifically, the selectivity of the reaction progressively shifted from telomer **2** (91%) to telomer **3** (80%) (Table 1, entries 1 and 6). In an aprotic solvent such as DMF, telomers **3** (76%) and **4** (24%) were obtained, while telomers **1** and **2** were not detected (Table 1, entry 7). Other aprotic-polar solvents such as DMA and *N*-methyl-2-pyrrolidone were also tested and provided similar results. Note that for telomers **1** and **2**, protonation occurred at a substituted carbon, while for telomers **3** and **4**, protonation occurred at a non-substituted carbon (see below for rationalization). The solvent effects were tested on other ligands driving the reaction in TFE, MeOH and DMF. For simple disphosphines dppe (**P5**) and dppp (**P6**), we observed the same general trend, that is, excellent selectivities towards telomers **2** and **3** in TFE and DMF solvents (up to 96% with dppp in both cases), respectively, and the preference for telomer **1** in MeOH (Table 1, entries 9-14). In addition, decreasing solvent acidity (increasing pKa) decreased the reaction yield, and heating was required to obtain good yields in the presence of DMF (Table 1, entries 8, 11 and 14).

The temperature mainly influenced the conversion and, to a lesser extent, the selectivity. When the reaction in TFE was heated at 50°C, selectivity to telomer **2** decreased, while cooling to -10°C increased the selectivity of **2** to 97%, although at the expense of the reaction rate. Conversely, when the reaction was performed in DMF at 80°C, the yield of telomer **3** increased strongly, while selectivity improved slightly (Table 1, entry 8). The use of bulky amines mainly influenced the reaction yield (Tables S7 and S10).

We also studied the influence of reaction parameters, such as Pd precursor, Pd loading, HNEt2/isoprene ratio and structure of amine, in both TFE and DMF as solvents (see SI, Tables S3-S12). The main results can be summarized as follows: 1) In the absence of ligands telomers were not formed in any solvent. 2) In TFE: i) all palladium precursors and phosphines tested provided high selectivity to 2 (84-92%); ii) an increase of palladium loading increased percentage of monomeric byproducts resulting from the addition of HNEt2 to isoprene; iii) when the HNEt2/isoprene ratio increased from 1 to 2.74 selectivity towards telomer **2** decreased from 91% to 36%, while increased the selectivity towards **1** from 9% to 48%; iv) the use bulky secondary amines provided excellent selectivity in telomer 2, but yield decreased. 3) In DMF: i) the telomer **3** was the major product with selectivities higher than 80% for a set of mono- and diphosphines; ii) the excess of Et2NH had no effect either on yield nor selectivity; iii) the use bulky secondary amines also provided excellent selectivities in telomer **3**, but also in this case, the yield decreased. 4) In anhydrous DMF, the reaction did not evolve.

In this context, we hypothesized that the selectivity of the other two telomers **1(TH)** and **4(HT)** may result from ligand control. Consequently, we screened structurally different ligands, including diphosphines (**P4-P12**), hemilabile P,N and P,O ligands (**P13**, **P16**), electron-poor phosphines (**P22-P24**) and sterically hindered monophosphines (**P2**, **P14, P15, P17-P21**) (Table 2, see full selectivity data in Supplementary Tables S11-S18).

Table 1. Solvent effect in the $Pd(OAc)_2$/ligand catalyzed telomerization of isoprene in the presence of Et_2NH.[a]

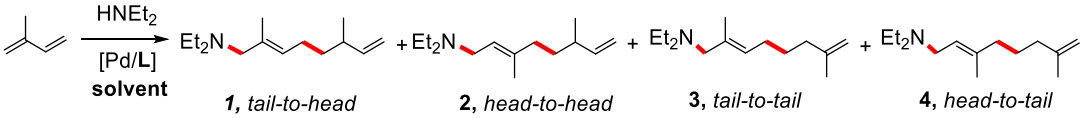

Entry	Ligand	Solvent	Yield Telom. (%)	Ratio 1 / 2 / 3 / 4	Ratio 1+2 /3+4
1	PPh_3 (**P1**)	TFE	86	09 / **91** / 0 / 0	100 : 0
2	PPh_3 (**P1**)	MeOH	99	51 / 29/ 19 / 1	80 : 20
3	PPh_3 (**P1**)	EtOH	93	39 / 08/ 27/ 26	47 : 53
4	PPh_3 (**P1**)	PrOH	46	24 / 04 / 36 / 36	28 : 72
5	PPh_3 (**P1**)	*i*PrOH	38	13 / 03 / 47 / 37	16 : 84
6	PPh_3 (**P1**)	*t*BuOH	8	02 / 03 / **80** / 15	5 : 95
7	PPh_3 (**P1**)	DMF	6	0 / 0 / **76** / 24	0 : 100
8	PPh_3 (**P1**)	DMF[b]	63	02 / 08 / **87** / 03	10 : 90
9	dppe (**P5**)	TFE	99	06 / **92** / 01 / 01	98 : 2
10	dppe (**P5**)	MeOH	84	62 / 12 / 21 / 05	74 : 26
11	dppe (**P5**)	DMF[b]	98	01 / 02 / **94** / 03	3 : 97
12	dppp (**P6**)	TFE	83	03 / **96** / 01 / 0	99 : 1
13	dppp (**P6**)	MeOH	82	64 / 16 / 17 / 03	80 : 20
14	dppp (**P6**)	DMF[b]	99	01 / 02 / **96** / 01	2 : 97

[a] Conditions: [Pd] (0.05 mmol), PPh3 (0.075 mmol), dppe and dppp (0.05 mmol), isoprene (10 mmol), Et2NH (10 mmol), solvent (2 mL), r.t., 24 h. [b] 80°C, Et3N (20 mmol).

The reaction was conducted at room temperature in a solvent with an intermediate pKa, such as methanol, in which telomer **1** had been preferably obtained (Table 1), and with $[Pd(\eta^3\text{-}C_3H_5)(COD)]BF_4$ as precursor.[19] Diphosphines, as well as electron poor monophosphines, provided low yields. In all cases, selectivities >50% to telomer **1** were obtained. Interestingly, using ligand **P14a**, a 92% selectivity to telomer **1** and 85% yield were obtained (Table 2). Extensive screening of solvents and reaction conditions using the $[Pd(\eta^3\text{-}C_3H_5)(COD)]BF_4$/**P14a** catalytic system always afforded telomer **1** as the major product. However, this ligand also afforded up to a 97% of telomer **2** when the reaction was performed in TFE.

Table 2. Screening of phosphine ligands in the Pd-catalysed telomerization of isoprene in MeOH. The yield of telomere mixture and only the selectivity for telomer 1 are shown.

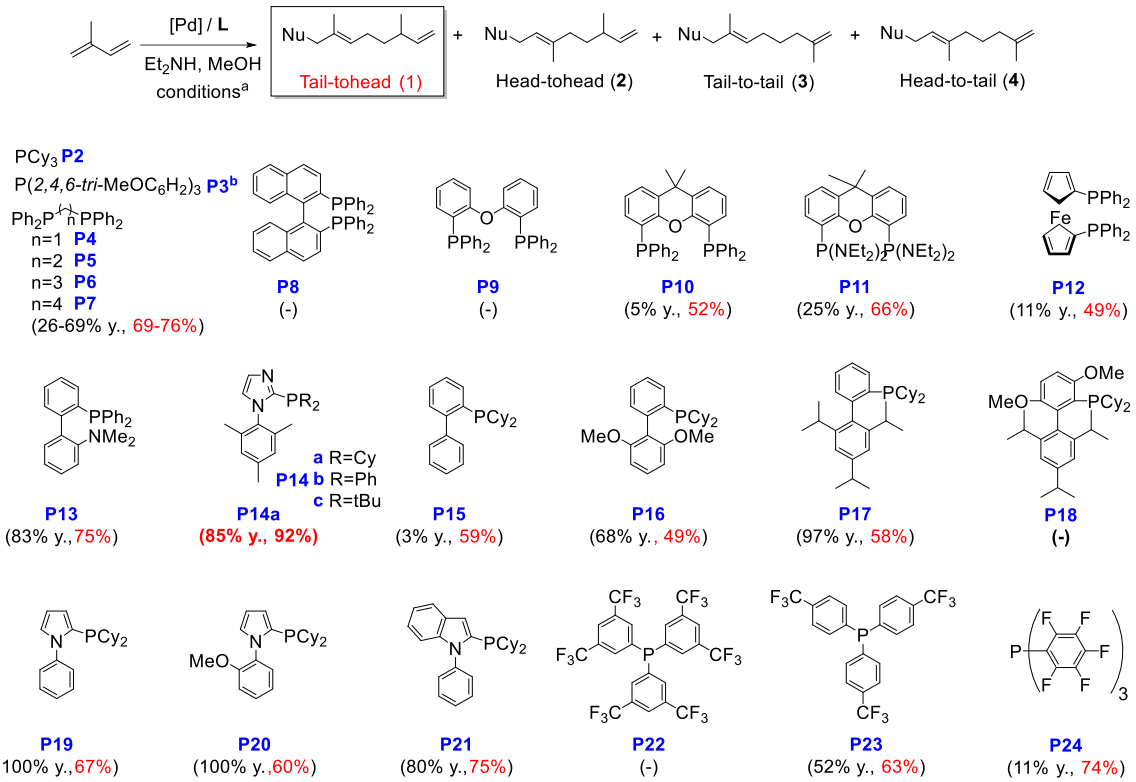

a Conditions: [Pd(η3-C3H5)(COD)]BF4 (0.05 mmol), ligand (0.05 mmol for diphosphines and 0.075 mmol for monophosphines), isoprene (10 mmol), Et2NH (9.6 mmol); MeOH (2 mL), r.t., 24h. b 95% sel. for telomer 2 (see ref. 19).

Intermediate detection and synthesis.

In the catalytic study, it was observed that the solvent pKa and ligands had a strong influence on both the activity and the selectivity of the reaction. To shed light on the mechanism we initially performed *in operando* ^{31}P NMR experiments using $Pd(OAc)_2/PPh_3$/isoprene in TFE and DMF. Under catalytic conditions a single signal was detected in each solvent at 26.5 ppm (TFE) and 26.3 ppm (DMF), which were initially attributed to intermediate complexes **8(HH)** and **8(TT)**, respectively (Scheme 3). To confirm the assignment of these complexes, we performed the independent synthesis of complexes **8**, following the procedure reported for butadiene (Scheme 3).[23,24,25,26] Thus, telomers **1-3**, obtained in the catalytic experiments, were first converted into the corresponding alcohols **5-7** (Scheme S1),[27] which were then treated with $Pd(dba)_2$ and triphenylphosphonium tetrafluoroborate, to obtain the corresponding complexes **8(TH)**, **8(HH)**, and **8(TT)**, which were characterized by single-crystal X-ray crystallography (Scheme 3, Figure S3, Tables S22, S23). In the 3 complexes, a distorted square planar geometry was observed where the 2,7-octadiene-1-yl ligands were bonded to Pd through an η^3-allylic fragment (C6, C7, C8) and a chelating η^2-olefin tail (C1, C2), with distinct orientations. The Pd-P bond lengths were very similar (*ca*. 2.32 Å) Complex **8 (T-T)** showed a *trans-cis-syn* configuration while **8 (H-H)** presented a 2-*trans-anti* configuration. The large steric demand of the octadienyl ligand is illustrated by the C1-Pd-C8 angle close to 180°.

The ^{31}P NMR data of complexes **8(HH)** and **8(TT)** were fully coincident with those obtained under catalytic conditions. Other possible reaction intermediates were also prepared (see SI) but were not detected under catalytic conditions.

In an additional experiment, complexes **8(TH)**, **8(HH)** and **8(TT)** were treated with Et_2NH (2 equiv./Pd) at room temperature for 30 minutes, and the corresponding telomers **1,2** and **3** were formed exclusively, confirming that the linear telomers were formed from the intermediates **8**, with retention of the regioselectivity. Complex **8(HH)** was also dissolved in DMF, which favors the formation of isomer **8(TT)**, heated to 60°C, and the evolution was monitored by ^{31}P NMR, but not new signals appeared after 6 h, discarding the interconversion between these isomers.

Scheme 3. Synthesis of complexes 8(TH), 8(HH), 8(TT), and their X-ray structure (BF_4^- anions are omitted for clarity, ellipsoids are drawn at 50% probability).

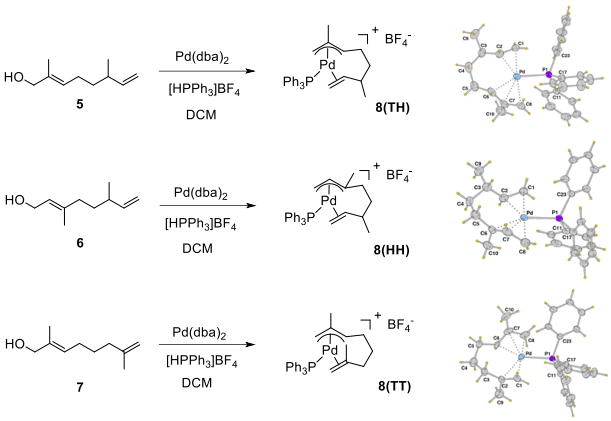

Computational characterization of the reaction mechanism.

To understand the factors controlling the selectivity in the palladium-catalyzed telomerization of isoprene with amines, we carried out a systematic DFT study under different solvent conditions and performed kinetic simulations.[28] Based on previous mechanistic studies on butadiene telomerization,[12-17] and in the characterization of catalytic intermediates described above, we proposed for the isoprene telomerisation with Et_2NH catalyzed by Pd/PPh_3 (**P1**), a catalytic cycle consisting of four main steps as illustrated by Figure 1: (1) isoprene coordination and oxidative coupling to form the allyl-alkyl intermediate $\mathbf{B_{P1}}$, (2) protonation of $\mathbf{B_{P1}}$ to yield the cationic allyl-alkene species $\mathbf{C_{P1}}$, (3) nucleophilic amine attack and reductive elimination giving Pd(0) complex $\mathbf{DH_{P1}}$, and (4) hydrogen abstraction to yield $\mathbf{D_{P1}}$. Figure 1 also shows the computed free-energy values for the four paths yielding the four telomers in TFE and *t*BuOH solvents.

Among the possible bi- and tricoordinated Pd(0) pre-catalyst species, the $Pd(PPh_3)_2$ complex turned out to be the most favorable energetically. From $Pd(PPh_3)_2$, the reaction is initiated by replacing one phosphine ligand and coordinating two isoprene units to the Pd(0) centre, yielding the $\mathbf{A_{P1}}$ structure. The carbon-carbon oxidative coupling in $\mathbf{A_{P1}}$ results in a η^3,η^3-diallyl-Pd(II) intermediate that rearranges to the more stable η^1,η^3-diallyl-Pd(II) complex $\mathbf{B_{P1}}$ via barrierless isomerization.[17] Palladium complexes with η^1,η^3-diallyl ligands have been experimentally isolated and characterized as a potential intermediate in Pd-catalyzed reactions with butadiene.[12] Note that the η^1- and η^3-allyl moieties can be formed from either the *tail* or the *head* sides of the original isoprene substrate, allowing us to distinguish between the **TH** and **HT** paths (Figure S7).

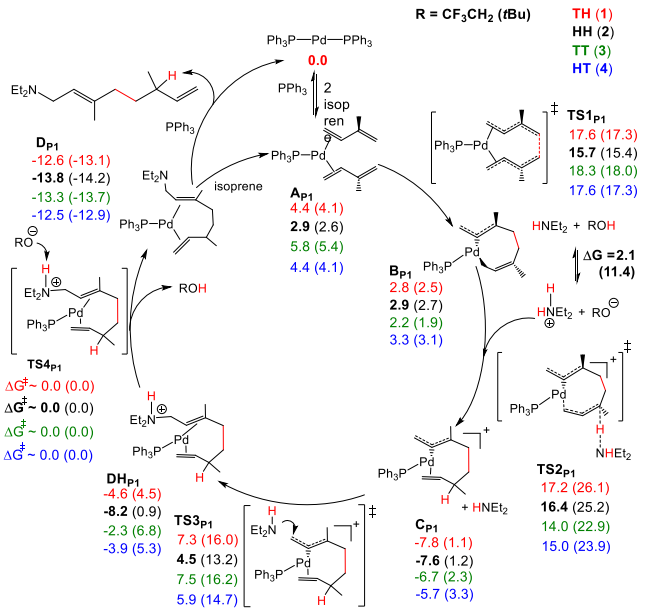

Figure 1. Computed catalytic cycle for the telomerization of isoprene with Et_2NH catalysed by the Pd/PPh_3 (**P1**) system, depicting path **HH**. Relative free-energy for **TH** (1st row, red), **HH** (2nd row, black), **TT** (3rd row, green) and **HT** (4th row, blue) in TFE and in *t*BuOH (shown in parenthesis).

The protonation of the intermediate $\mathbf{B_{P1}}$ gives the observed cationic Pd(II) intermediate $\mathbf{C_{P1}}$. Direct protonation by the secondary amine Et_2NH via external attack or via previous coordination to palladium can be discarded because of the high energy associated with the processes (> 40 kcal·mol^{-1}). Alternatively, as previous DFT studies on butadiene isomerization suggests,[17] the $Et_2NH_2^+$ species, resulting from deprotonation of the acidic hydrogens of the solvents, can act as a proton source (Figure 1). We selected the two alcohol solvents with the most extreme acidity, TFE and *t*BuOH. The free energy cost associated with the deprotonation process (ΔG = 2.1 and 11.4 kcal·mol^{-1}, respectively) was estimated using the experimental pKa values (Table S24). Thus, the calculation of the overall free-energy barrier for protonation can be divided into three additive steps avoiding the calculation of charge separation processes: (1) the free energy cost for deprotonation derived from experimental pKa values, (2) the entropic term associated with the formation of the hydrogen-bonded adduct between $Et_2NH_2^+$ and $\mathbf{B_{P1}}$ assuming that the hydrogen bonds are similar to those set with the solvent, and consequently, the associated enthalpy can be set to zero, and (3) the free energy cost for the hydrogen transfer from the hydrogen-bonded adduct. Note that the protonation barrier depends strongly on the acidity of the solvent; the higher the pKa is, the larger the energy barrier (1.4 Kcal/mol per pKa unit), resulting in the same increase for all isomeric paths. This reaction step is clearly exergonic, leading to the low-energy intermediate $\mathbf{C_{P1}}$, in full agreement to analogous experimentally characterized complexes **8**.

Once the Pd complex is activated via protonation ($\mathbf{C_{P1}}$), there is an external nucleophilic attack by Et_2NH at the π-allyl moiety to form the observed linear telomer with moderate free energy barriers. Then, the resulting quaternary amine in $\mathbf{DH_{P1}}$ is deprotonated by the conjugated base of the solvent (alkoxide) present in the medium to yield the product coordinated to the Pd(0) centre and regenerate the solvent (Figure 1). In this case, the analysis of deprotonation of DH_{P_1} by non-solvated alkoxide molecule indicates a barrierless process. Importantly, from $\mathbf{C_{P1}}$ intermediates, the forward barriers to give the final product are significantly lower in energy than those in the reverse reaction to give $\mathbf{B_{P1}}$, further supporting the irreversibility of protonation.

The overall catalytic cycle depicted in Figure 1 reveals two different kinetic scenarios (I and II) for acidic TFE and non-acidic tBuOH solvents. In TFE, the protonation step is fast and irreversible, making oxidative addition the selectivity-determining step (kinetic *scenario I*). Accordingly, assuming a Boltzmann distribution of the relative energies of transition states for oxidative addition, for $\mathbf{TS1_{P_1}}$, the predicted isomer distribution is 4%, 91%, 1%, and 4% for telomers **1**, **2**, **3** and **4**, respectively, in excellent agreement with the experimental values (Table 1, entry 1). The kinetic modelling using the energy parameters of Figure 1 gives the same isomer distribution, indicating that the high concentration of solvent as reactant speeds up the protonation step, in a scenario in which the transition states ($\mathbf{TS2_{P_1}}$) have very close energy to those for C-C coupling ($\mathbf{TS1_{P_1}}$).

For the low acidic *t*BuOH solvent, the free-energy cost associated with its deprotonation process rises, resulting in a higher-laying transition states for protonation ($\mathbf{TS2_{P_1}}$). Therefore, we might have a different kinetic scenario, slow protonation and reversible oxidative coupling (kinetic *scenario II*), in which protonation is the selectivity-determining step. In this case, the calculated isomer distribution from the relative free-energies of $\mathbf{TS2_{P_1}}$ (0.4%, 2%, 83% and 15% for telomers **1**, **2**, **3** and **4**), respectively, also fits very well with the experimental results (Table 1, entry 6). Another consequence of reducing solvent acidity is the increase in the overall free-energy barrier by ~6.5 kcal·mol^{-1}, which agrees with the observed decrease in reaction rate from TFE to *t*BuOH.

Origin of the solvent control of selectivity.

The decrease in solvent acidity causes a continuous shift in the selectivity-determining step from oxidative addition to protonation, therefore, the features of both steps need to be analyzed separately to understand the origin of the selectivity. In the acidic solvent TFE (kinetic *scenario I*), the preferred path **HH** proceeds via coordination of two isoprenes to Pd through the *tail* moieties, adopting an alternate conformation that avoids steric repulsion between the two methyl groups (Figure 2) in the corresponding transition state $\mathbf{TS1_{P_1}}$. The other possible coordination modes involve the isoprene interaction with Pd through one *tail* and one *head* moieties (**TH** and **HT** paths) and through both *head* moieties (**TT** path). The energy analysis of the different paths in oxidative addition (Figures 1 and 2) indicates that bringing the substituted alkene fragment (*head*) to the coordination sphere of palladium has a negative impact on the stability of the $\mathbf{A_{P_1}}$ and $\mathbf{TS1_{P_1}}$ species because of the increase of steric hindrance.

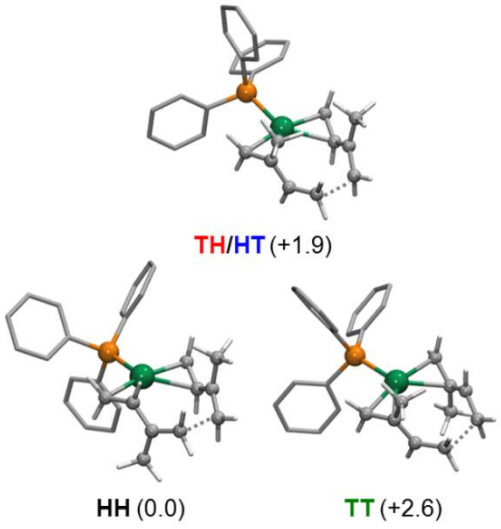

Figure 2. Molecular structures of the transition states for oxidative coupling of the two isoprenes ($\mathbf{TS1_{P_1}}$) and relative free-energies in kcal·mol^{-1}.

For the low acidity solvent *t*BuOH (kinetic *scenario II*), we analysed the intermediate $\mathbf{B_{P_1}}$, which must be protonated at the alkene, γ-carbon of the η^1-σ-allyl moiety, to yield the intermediate $\mathbf{C_{P_1}}$. Following Markovnikov's rule for the addition to non-symmetric alkenes, protonation is favored at the less substituted carbon, as displayed by the **TT** (**3**) and **HT** (**4**) paths, which show lower free-energy barriers than the **TH** (**1**) and **HH** (**2**) isomers (Figure 3). Accordingly, the analysis of charge distribution in $\mathbf{B_{P_1}}$ demonstrates that Cγ is more negatively charged for isomers **TT** (**3**) and **HT** (**4**). Finally, we attribute the preference of the **TT** path over the **HT** path to the steric factors associated with the different substitution pattern of the η^3-π-allyl moiety, as manifested in their relative energies in the $\mathbf{B_{P_1}}$ intermediate.

The control of selectivity by the solvent is illustrated in Figure 4, which displays the evolution of isomer distribution as a function of the pKa values derived from kinetic modelling. Note that pKa values are very sensitive to the media in which they are determined. In this case, using the average values between the tabulated pKa values in aqueous media and their values for autoprotolysis, we found an excellent fitting of the kinetic model to the experimental selectivity, particularly the percentage of evolution from **1+2** to **3+4** (Figure 4 and SI for detailed discussion on pKa values). The simulations show that increasing the pKa value,

reduces the percentage of isomer **2** exponentially, while the percentage of isomer **3** increases exponentially.

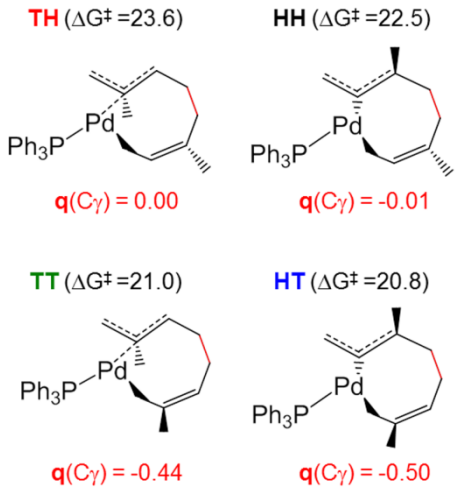

Figure 3. Electrostatic based atomic charges (a.u.) for the γ carbon of the η¹-σ-allyl moiety of the $\mathbf{B_{P_1}}$ intermediate and free-energy barriers (ΔG‡) for the protonation step in *t*BuOH solvent in kcal·mol⁻¹.

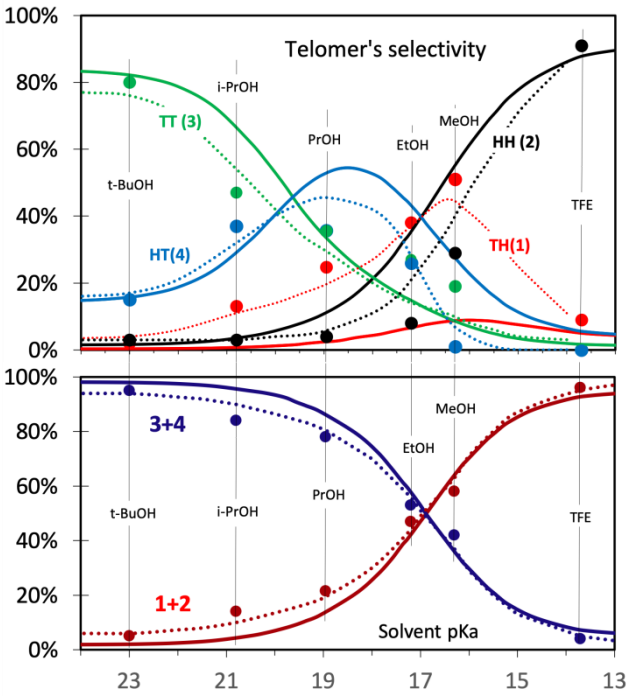

Figure 4. Microkinetic modelling of the percentage evolution for each isomer, top, and of the percentage evolution for (**1**+**2**) and (**3**+**4**), bottom, as a function of the solvent pKa. Dots and dotted lines correspond to experimental values, while solid lines correspond to simulated values.

Isomers **1** and **4** follow a bell-shaped distribution with maximums at intermediate pKa values. At intermediate pKa values, the selectivity is not governed by a single step, oxidative coupling ($\mathbf{TS1_{P_1}}$) or protonation ($\mathbf{TS2_{P_1}}$), but the slowest reaction step depends on the isomer, leading to a more complex kinetic scenario. Thus, our simulations for **3** and **4** are able to reproduce the shape and the position of

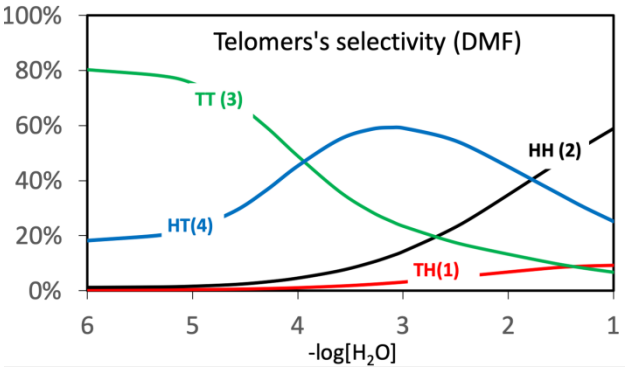

Figure 5. Microkinetic modelling of the percentage evolution for each isomer as a function of the amount of water impurities in DMF solvent. Initial simulated conditions: $Pd(PPh_3)_2$ (0.075 mmol), isoprene (10 mmol), Et_2NH (10 mmol), solvent (2 mL), 25ºC, 24 h.

the evolution curve but not the quantitative proportions of the two isomers.

Another striking observation is that aprotic solvents such as DMF provide **3** as a major isomer with a low yield, even when the acid-base equilibrium between the solvent and the amine is not possible. Here we propose that water impurities of the solvent catalyze the reaction by generating $Et_2NH_2^+$ species in a similar way as TFE and tBuOH.[29] Figure 5 plots the simulated variation in isomer distribution as a function of water content obtained by kinetic modelling using the energy parameters from the DFT calculations (Figure S9). At low water concentration (< 10^{-4} M), we reproduced **3** as a major isomer; and in this case, we note that including diffusion energy barrier in the kinetic model would also predict isomer **3** for larger amount of water. More interestingly however, the percentage evolution of the isomers as a function of protic solvent content is analogous to that as a function of solvent pKa (compare Figures 4 and 5). Additional experiments reducing systematically TFE amount confirm the shift of selectivity from **2** to **3** and the reduction of catalytic activity (see Table S19), in full agreement with the proposed kinetic model.

Origin of ligand control of selectivity.

Experimental ligand screening in methanol (Table 2, Tables S11-S18) has shown that using the sterically hindered monophosphine **P14a**, the reaction can be directed towards isomer **1**. Interestingly, the same catalytic system gives isomer **2** as the major product in TFE, while the selectivity towards **1** is somewhat reduced in *t*BuOH (see Table S17). We computed the full catalytic cycle for the Pd/**P14a** catalyst (Figure S10), and Figure 6 shows the molecular structures of the transition states for the key protonation step ($\mathbf{TS2_{P_{14}}}$). From the PPh_3 to **P14a** ligand, protonation at the substituted γ-carbon through **TH** (**1**) path be-

comes energetically preferred, indicating that the selectivity in the protonation step is not electronically but sterically controlled.

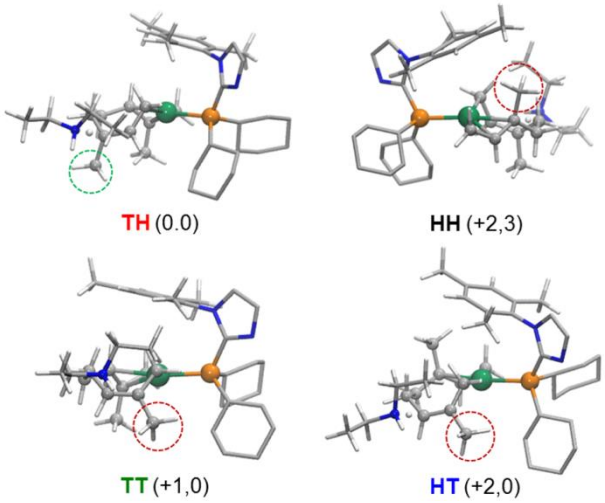

Figure 6. Molecular structures of the transition states for protonation (**TS2**$_{P14}$) by the Pd/**P14a** catalyst and relative free-energies in kcal·mol^{-1}.

The conformation of the **P14a** ligand places the mesityl substituent of the imidazole ring over the metal centre (Figures 6 and S11), hindering one coordination site and blocking ligand rotation around the Pd-phosphine bond, which provides more rigid Pd-ligand scaffold. Thus, in the **TT** (**3**) and **HT** (**4**) paths, the methyl substituent at the β-carbon of the η^1-σ-allyl moiety suffers a repulsive steric interaction with one cyclohexyl substituent of the phosphine ligand, while in the **HH** (**2**) path, the alternated conformation of the two methyl substituents results in a destabilizing interaction between the methyl of the π-allyl moiety and the mesityl group of the phosphine (Figures 6 and S11). The calculated isomer distributions from the relative free-energies of **TS2**$_{P14}$ (0.0, +2.3, +1.0, 2.0 kcal mol^{-1} in Figure 6) were 81%, 2%, 14% and 3% for **1**, **2**, **3** and **4**, respectively, while those from **TS1**$_{P14}$ (+3.1, 0.0, +8.5 and +3.1 kcal mol^{-1} in Figure S12) were 0.5%, 99%, 0% and 0.5%, respectively. Thus, in low-acidity *t*BuOH solvent (76% of **1**), the selectivity is governed by the protonation step (**TS2**$_{P14}$) favouring isomer **1**, while in high-acidity TFE solvent (93% of **2**) it is governed by oxidative C-C coupling (**TS1**$_{P14}$). For MeOH solvent (92% of **1**), we propose that protonation is still the selectivity-determining step but the **TS2**$_{P14}$ species become closer in energy to **TS1**$_{P14}$, in which the **TT** (**3**) path is sterically blocked (relative free-energy of +8.5 kcal mol^{-1}), increasing the proportion of **1** at the expense of **3**.

CONCLUSION

A combined experimental and computational study showed that solvent and ligand are both responsible for controlling the selectivity in the isoprene telomerization catalyzed by palladium complexes. The solvent control occurs as a function of its pKa, which is responsible of a continuous shift of the selectivity-determining step. For acidic solvents (TFE), the protonation step is fast and irreversible (kinetic scenario I), and the selectivity is governed by the C-C oxidative coupling. Under these conditions, the catalyst favours the least sterically demanding **HH** path (telomer **2**), which minimizes substrate-substrate and ligand-substrate repulsive interactions. As solvent acidity decreases (e.g. *t*BuOH), the protonation step becomes slower and more influential in the selectivity (kinetic scenario II), favoring the formation of telomer **3** (**TT**), which is more easily protonated at the non-substituted carbon of the η^1,η^3-diallyl. The ligand **P14a** directs the selectivity towards the telomer **1** (**TH**) in moderately acidic solvents though the steric control of the protonation step via the mesityl substituent of the imidazole ring, which generates a more hindered and rigid metal-ligand scaffold. As a consequence of this study, telomers **1-3** were obtained in high yields and selectivities >90% using palladium catalysts.

ASSOCIATED CONTENT

The Supporting Information is available free of charge at https://pubs.acs.org/

Synthetic procedures, testing parameters tables, intermediates detection and synthesis, NMR spectra, details of quantum-chemical calculations and kinetic simulations, energy parameters of computed catalytic cycles, , including calculated catalytic cycles in DMF and for ligand **14a** 3D representations of selected intermediates and transition states, and DFT-optimized Cartesian coordinates (PDF).

AUTHOR INFORMATION

Corresponding Authors

Sergio Castillon – *Departament de Química Analítica i Orgànica, Universitat Rovira i Virgili, C/Marcel·lí Domingo 1, 43007 Tarragona, Spain;*

CTQC/Eurecat-UTQ, C/Marcel·lí Domingo 2, building N5, 43007 Tarragona, Spain https://orcid.org/0000-0002-0690-7549; Email: *sergio.castillon@urv.cat.*

Jorge J. Carbó – *Departament de Química Física i Inorgànica, Universitat Rovira i Virgili, C/Marcel·lí Domingo 1, 43007 Tarragona, Spain; orcid.org/0000-0002-3945-6721*; Email: *j.carbo@urv.cat.*

Authors

Jordi Colavida – *CTQC/Eurecat-UTQ, C/Marcel·lí Domingo 2, building N5, 43007 Tarragona, Spain*

José J. Lleberia – *Departament de Química Física i Inorgànica, Universitat Rovira i Virgili, C/Marcel·lí Domingo 1, 43007 Tarragona, Spain*

Antoni Salom-Català – *Departament de Química Física i Inorgànica, Universitat Rovira i Virgili, C/Marcel·lí Domingo 1, 43007 Tarragona, Spain*

Aitor Gual – *CTQC/Eurecat-UTQ, C/Marcel·lí Domingo 2, building N5, 43007 Tarragona, Spain*

Ana Collado – *International Flavors and Fragrances, Av/Felipe Klein 2, 12580 Benicarló, Spain*

Ennio Zangrando – *Dipartimento di Scienze Chimiche e Farmaceutiche, University of Trieste, Via L. Giorgieri 1, 34127 Trieste, Italy*

Josep M. Ricart – *Departament de Química Física i Inorgànica, Universitat Rovira i Virgili, C/Marcel·lí Domingo 1, 43007 Tarragona, Spain*

Cyril Godard – *Departament de Química Física i Inorgànica, Universitat Rovira i Virgili, C/Marcel·lí Domingo 1, 43007 Tarragona, Spain*

Carmen Claver – *Departament de Química Física i Inorgànica, Universitat Rovira i Virgili, C/Marcel·lí Domingo 1, 43007 Tarragona, Spain.*
CTQC/Eurecat-UTQ, C/Marcel·lí Domingo 2, building N5, 43007 Tarragona, Spain

Complete contact information is available at: https://pubs.acs.org/

Author Contributions

The manuscript was written through contributions of all authors.

Notes

The authors declare no competing financial interest.

ASSOCIATED CONTENT

The Supporting Information is available free of charge at https://pubs.acs.org/

Synthetic procedures, testing parameters tables, intermediates detection and synthesis, NMR spectra, details of quantum-chemical calculations and kinetic simulations, energy parameters of computed catalytic cycles, , including calculated catalytic cycles in DMF and for ligand **14a** 3D representations of selected intermediates and transition states, and DFT-optimized Cartesian coordinates (PDF).

ACKNOWLEDGMENT

Dedicated to the memory of Professor Kilian Muñiz (ICIQ, Tarragona, Spain). This work was financed by IFF Inc. (USA). JC thanks IFF Inc. for a PhD scholarship. We thank Dr. Richard Boden (IFF) for fruitful discussions. We thank Acció (Gencat) for financial support (TELCAT and ILCATSIN) projects. We also thank the Spanish Ministry of Science (CTQ2017-89750-R, CTQ2016-75016-R, AEI/FEDER, UE, and PGC2018-100780-B-100), the Generalitat de Catalunya (2017SGR629), and Analytical Services of Universitat Rovira i Virgili for support.

REFERENCES

1. Smutny, E. J. Oligomerization and Dimerization of Butadiene under Homogeneous Catalysis. Reaction with Nucleophiles and the Synthesis of 1,3,7-Octatriene. *J. Am. Chem. Soc.* **1967**, *89*, 6793–6794.
2. Takahashi, S.; Shibano, T.; Hagihara, N. The telomerization of butadiene by palladium complex catalysts. *Tetrahedron Lett.* **1967**, *8*, 2451–2453.
3. Fassbach, T. A.; Vorholt, A. J.; Leitner, W. The Telomerization of 1,3-Dienes – A Reaction Grows Up. *ChemCatChem* **2019**, *11*, 1153–1166.
4. Herrmann, N.; Vogelsang, D.; Behr, A.; Seidensticker, T. Homogeneously Catalyzed 1,3-Diene Functionalization – A Success Story from Laboratory to Miniplant Scale. *ChemCatChem* **2018**, *10*, 5342–5365.
5. Behr, A.; Neubert, P. *Applied Homogeneous Catalysis*, Wiley-VCH, 2012.
6. Behr, A.; Becker, M.; Beckmann, T.; Johnen, L.; Leschinski, J.; Reyer, S. Telomerization: Advances and Applications of a Versatile Reaction. *Angew. Chem. Int. Ed.* **2009**, *48*, 3598–3614.
7. Consiglio, G. Waymouth, R. M. Enantioselective homogeneous catalysis involving transition metal-allyl intermediates. *Chem. Rev.* **1989**, *89*, 257–276.
8. Clement, N. D.; Routaboul, L.; Grotevendt, A.; Jackstell, R.; Beller, M. Development of Palladium–Carbene Catalysts for Telomerization and Dimerization of 1,3-Dienes: From Basic Research to Industrial Applications. *Chem. Eur. J.* **2008,** *14*, 7408–7420.
9. Tschan, M. J. L.; García-Suárez, E. J.; Freixa, Z.; Launay, H.; Hagen, H.; Benet-Buchholz, J.; van Leeuwen, P. W. N. M. Efficient Bulky Phosphines for the Selective Telomerization of 1,3-Butadiene with Methanol. *J. Am. Chem. Soc.* **2010**, *132*, 6463–6473.
10. Harkal, S.; Jackstell, R.; Nierlich, F.; Ortmann, D.; Beller, M. Development of a highly selective and efficient catalyst for 1,3-butadiene dimerization. *Org. Lett.*, **2005**, *7*, 541–544.
11. van Leeuwen, P. W. N. M.; Clément, N. D.; Tschan, M. J. L. New processes for the selective production of 1-octene. *Coord. Chem. Rev.* **2011**, *255*, 1499–1517.
12. Benn, R.; Jolly, P. W.; Mynott, R.; Schenker, G. Intermediates In the Palladium-Catalyzed Reactions of 1,3-Dienes.1. (η^3,η^3-Dodecatrienediyl)palladium, [Pd(η^3,η^3-$C_{12}H_{18}$)]. *Organometallics* **1985**, *4*, 1136–1138.
13. Benn, R., Jolly, P. W., Mynott, R., Raspel, B., Schenker, G., Schick, K. P.; Schroth, G. Intermediates in the Palladium-Catalyzed Reactions of 1,3-Dienes. 2. Preparation and Structure of (η^1,η^3-octadienediyl)palladium Complexes. *Organometallics* **1985**, *4*, 1945–1953.
14. Jolly, P. W.; Mynott, R.; Raspel, B.; Schick, K. P. Intermediates in the Palladium-Catalyzed Reactions of 1,3-Dienes. 3. The Reaction of (η^1,η^3-octadienediyl)palladium Complexes with Acidic Substrates. *Organometallics* **1986**, *5*, 473–481.
15. Völkl, L.; Recker, S.; Niedermaier, M.; Kiermaier, S.; Strobel, V.; Maschmeyer, D.; Cole-Hamilton, D.; Marquardt, W.; Wasserscheid, P.; Haumann, M. Comparison between phosphine and NHC-modified Pd catalysts in the telomerization of butadiene with methanol – A kinetic study combined with model-based experimental analysis. *J. Catal.* **2015**, *329*, 547–559.
16. Huo, C.-F; Jackstell, R.; Beller, M.; Jiao, H. Mechanistic study of palladium-catalyzed telomerization of 1,3-butadiene with metanol. *J. Mol. Model.* **2010**, *16*, 431–436.
17. Jabri, A.; Budzelaar, P. H. M. DFT Study of Pd(PMe_3)/NMe_3-Catalyzed Butadiene Telomerization of Methanol *Organometallics*, **2011**, *30*, 1374–1381.
18. Jackstell, R.; Grotevendt A.; Michalik, D.; El Firdoussi, L.; Beller M. Telomerization and dimerization of isoprene by *in situ* generated palladium–carbene catalysts. *J. Organomet. Chem.* **2007**, *692*, 4737–4744.
19. Maddock, S. M., Finn, M. G. Palladium-Catalyzed Head-to-Head Telomerization of Isoprene with Amines. *Organometallics* **2000**, *19*, 2684-2689.
20. Leca, F.; Réau, R. 2-Pyridyl-2-phospholenes: New P,N ligands for the palladium-catalyzed isoprene telomerization. *J. Catal.* **2006**, *238*, 425–429.
21. Keim, W.; Kurtz, K.-R.; Röper, M. Palladium catalyzed telomerization of isoprene with secondary amines and conversion of the resulting terpene amines to terpenols. *J. Mol. Catal.* **1983**, *20*, 129–138.
22. Castillon, S.; Claver, C.; Godard, C.; Colavida, J.; Collado, A.M.; Boden, R. W.; Amorelli, B. Process for the telomerization of conjugated alkadienes. EP 3222610 (2017).
23. Hausoul, P. J. C.; Parvulescu, A. N.; Lutz, M.; Spek, A. L.; Bruijnincx, P. C. A.; Weckhuysen, B. M.; Klein Gebbink, R. J. M. Facile Access to Key Reactive Intermediates in the Pd/PR_3-Catalyzed Telomerization of 1,3-Butadiene. *Angew. Chem. Int. Ed.* **2010**, *49*, 7972–7975.
24. Storzer, U.; Walter, O.; Zevaco, T.; Dinjus, E. (Cyclohexylmethylphenylphosphine)[(1-η^1:6−8-η^3)-octa-2,6-diene-1,8-

diyl]palladium(II)] as a Model for Key Intermediates in Enantioselective Reactions of 1,3-Butadiene Catalyzed by Palladium(0). *Organometallics* **2005**, *24*, 514–520.

25. Hausoul, P. J. C.; Parvulescu, A. N.; Lutz, M.; Spek, A. L.; Bruijnincx, P. C. A.; Gebbink, R. J. M. K.; Weckhuysen, B. M. Mechanistic Study of the Pd/TOMPP-Catalyzed Telomerization of 1,3-Butadiene with Biomass-Based Alcohols: On the Reversibility of Phosphine Alkylation. *ChemCatChem* **2011**, *3*, 845–852.
26. Urbin, S. A.; Pintauer, T.; White, P.; Brookhart, M. Synthesis, characterization, and reactivity of (π-allyl)palladium(II) wrap-around complexes with 1,3-dienes. *Inorg. Chim. Acta* **2011**, *369*, 150–158.
27. Antonsson, T.; Malmberg, C.; Moberg, C. Regio- and stereoselective palladium-catalyzed functionalizations of dienes. Synthesis of (±)-sativene. *Tetrahedron Lett.* **1988**, *29*, 5973–5974.
28. DFT calculations were performed with Gaussian09 using M06 functional. The basis set was lanl2dz supplemented with d and f shells for P and Pd atoms, respectively, and 6-31g(d,p) for the rest of main group elements. Energies include free energy corrections at concentration of 1 M and 298.15 K and the different solvent effects by IEF-PCM continuum solvent model. The kinetic simulations were carried out with Acuchem software and rate constants were calculated using the Eyring approximation and transition state theory. See the Supporting Information for details.
29. For an example, see: García-López, D.; Civit, M. G.; Vogels, C. M.; Ricart, J. M.; Westcott, S. A.; Fernández, E.; Carbó, J. J. Understanding the mechanism of transition metal free *anti* addition to alkynes: the selenoboration case. *Catal. Sci. Technol.* **2018**, *8*, 3617–3628.

Table of Contents graphic